SHORT REPORTS

Cathepsin Z is a conserved susceptibility factor underlying tuberculosis severity

Rachel K. Meade[1,2,☉], **Oyindamola O. Adefisayo**[1☉], **Marco T. P. Gontijo**[1☉],
Summer J. Harris[1], **Charlie J. Pyle**[1], **Kaley M. Wilburn**[1], **Alwyn M. V. Ecker**[1],
Erika J. Hughes[1,2], **Paloma D. Garcia**[1], **Joshua Ivie**[3], **Michael L. McHenry**[4],
Penelope H. Benchek[4], **Harriet Mayanja-Kizza**[5], **Jadee L. Neff**[6], **Dennis C. Ko**[1,2],
Jason E. Stout[7], **Catherine M. Stein**[4,8], **Thomas R. Hawn**[3], **David M. Tobin**[1,2,9],
Clare M. Smith [ID][1,2]*

1 Department of Molecular Genetics and Microbiology, Duke University, Durham, North Carolina, United States of America, 2 University Program in Genetics and Genomics, Duke University, Durham, North Carolina, United States of America, 3 Department of Medicine, University of Washington, Seattle, Washington, United States of America, 4 Department of Population and Quantitative Health Sciences, Case Western Reserve University, Cleveland, Ohio, United States of America, 5 Uganda-CWRU Research Collaboration and Department of Medicine, School of Medicine, Makerere University, Kampala, Uganda, 6 Department of Pathology, Duke University, Durham, North Carolina, United States of America, 7 Division of Infectious Disease and International Health, Department of Medicine, Duke University Medical Center, Durham, North Carolina, United States of America, 8 Department of Medicine, Case Western Reserve University, Cleveland, Ohio, United States of America, 9 Department of Integrative Immunobiology, Duke University, Durham, North Carolina, United States of America

☉ These authors contributed equally to this work.
* clare.m.smith@duke.edu

Abstract

Tuberculosis (TB) outcomes vary widely, from asymptomatic infection to mortality, yet most animal models do not recapitulate human phenotypic and genotypic variation. The genetically diverse Collaborative Cross mouse panel models distinct facets of TB disease that occur in humans and allows identification of genomic loci underlying clinical outcomes. We previously mapped a TB susceptibility locus on mouse chromosome 2. Here, we identify cathepsin Z (*Ctsz*) as a lead candidate underlying this TB susceptibility and show that *Ctsz* ablation leads to increased bacterial burden, pulmonary inflammation and decreased survival in mice. *Ctsz* disturbance within murine macrophages enhances production of chemokine (C-X-C motif) ligand 1 (CXCL1), a known biomarker of TB severity. From a Ugandan household contact study, we identify significant associations between *CTSZ* variants and TB disease severity. Finally, we examine patient-derived TB granulomas and report CTSZ localization within granuloma-associated macrophages, placing human CTSZ at the host–pathogen interface. These findings implicate a conserved CTSZ-CXCL1 axis in humans and genetically diverse mice that mediates TB disease severity.

Introduction

Mycobacterium tuberculosis (*Mtb*), the causative agent of tuberculosis (TB), is a prolific obligate pathogen that has threatened human health for millennia [1]. Through centuries of coevolution, human hosts have developed a plethora of immunological mechanisms in response to *Mtb* infection [2]. Such host-bacterial interactions give rise to a spectrum of disease states, ranging from subclinical infection to fulminant disease [3]. The disease severity experienced by an individual is intricately connected to their genetic background. For example, monozygotic twins are at a demonstrably higher risk for TB concordance than dizygotic twins, highlighting shared genetic identity as a contributor to TB disease outcomes [4–6]. Human genome-wide association studies (GWAS) conducted in impacted geographic regions have also identified polymorphisms that modulate host TB immunity [7–13], indicating numerous immunological pathways involved in *Mtb* susceptibility.

One such gene is cathepsin Z (*CTSZ*), which has been associated with TB susceptibility in independent human studies conducted across Africa. *CTSZ* encodes a lysosomal cysteine protease with a known structure and several reported cellular functions [14–22]. The link between single-nucleotide polymorphisms (SNPs) in *CTSZ* and human TB susceptibility was first established by sibling pair analysis in South African and Malawian populations and independent case-control studies in West Africa [23]. These findings were further validated in a South African case-control study [24] and in a Ugandan GWAS [25] and subsequent household contact study [26]. *CTSZ* is primarily expressed by monocytes and macrophages [27–30] and participates in central immune functions, including dendritic cell maturation [31] and lymphocyte propagation and migration [32,33]. Although in vitro work has been undertaken to study the role of CTSZ in macrophage-driven protection against mycobacteria [34,35], *CTSZ*-linked TB susceptibility has not been explored in vivo. The functional role of CTSZ during *Mtb* infection remains unknown, despite growing genetic evidence of its association with TB disease outcomes.

Studying the mechanisms that underlie *CTSZ*-linked susceptibility in humans is complex [36]. Humans are outbred, and genetic studies of human cohorts must navigate the inherent challenges of natural genetic variation. Moreover, the low- and middle-income countries that harbor 80% of the global TB burden face challenges in and outside of the healthcare sector that complicate TB diagnosis, research, and treatment [37]. The connection between TB severity and host background is not uniquely human. In classic *Mtb* studies measuring postinfection survival, inbred mice have repeatedly illustrated the heritability of TB susceptibility [38,39]. Combining reproducibility with a limited range of genetic variation, classical inbred laboratory mice have served as tractable models that demonstrate the vital impact of host genetic background on *Mtb* pathogenesis. However, because inbred mice are nearly genetically identical within strain [40], studies leveraging standard inbred strains omit the contributions of natural host genetic diversity to TB pathogenesis. Recombinant inbred panels like the biparental BXD [41–44] and octoparental Collaborative Cross (CC) [45–47] systematically model host genetic variation, allowing insight into

a spectrum of immune profiles without compromising the reproducibility of inbred strains [48]. We previously reported *Mtb* infection screens of BXD [49] and CC [50] recombinant inbred strains, leveraging these diverse mammalian panels to expand the range of known TB disease complexes and host-pathogen interactions modeled by mice. Using a quantitative trait locus (QTL) mapping approach across a cohort of 52 CC genotypes, we identified a QTL on chromosome 2 (174.29–178.25Mb) significantly associated with *Mtb* burden. Genetic inheritance from NOD/ShiLtJ (NOD), a CC panel founder, at the *Tuberculosis ImmunoPhenotype 5* (*Tip5*) QTL predicted elevated bacterial burden. CC strains that inherited the susceptible *Tip5* variant (*Tip5^S*) from NOD succumbed to severe TB prior to the study endpoint. We therefore sought to determine which genes found within the *Tip5* interval could contribute to *Mtb* susceptibility in *Tip5^S* CC strains.

Here, we show that CC strains harboring the *Tip5^S* locus produce lower levels of CTSZ protein while exhibiting higher bacterial burden than B6 mice following aerosol infection, validating *Tip5* as a susceptibility locus from the large-scale CC cohort screen. We report the first in vivo *Mtb* infections of mice lacking *Ctsz* (*Ctsz^−/−*). We find that *Ctsz* ablation on a B6 background results in increased *Mtb* burden and an increased risk of mortality following infection. Moreover, *Ctsz^−/−* mice overproduce CXCL1, a biomarker of active TB [51], at both acute and chronic timepoints. In *Ctsz^−/−* bone marrow-derived macrophages (BMDMs), we find that CXCL1 is rapidly induced following mycobacterial infection. Leveraging published transcriptional data from genetically diverse mice, humans, macaques, and zebrafish, we find cathepsin Z expression is highest in macrophages following infection. We combine these findings with recent data from a Ugandan patient cohort, highlighting five variants in *CTSZ* as correlates of TB severity. Finally, we identify the presence of CTSZ in CD68+ macrophages within patient-derived pulmonary granulomas, revealing that CTSZ is produced at the host-pathogen interface in human lungs. Collectively, this work establishes genetic variation in cathepsin Z as a determinant of TB disease outcomes and places human CTSZ in a vital position within the pulmonary microenvironment to impact TB outcomes.

Results

Comparative transcriptional analysis to prioritize candidate genes within the *Tip5* locus

We previously reported the *Tip5* QTL (Chr2, 174.29–178.25Mb) as a TB susceptibility locus across the genetically diverse CC panel [50]. To identify gene candidates within *Tip5*, we leveraged published transcriptomic data from *Mtb*-infected mammalian lungs [52,53] (Fig 1A). Within the *Tip5* interval, cathepsin Z (*Ctsz*; alternative names: cathepsin X, cathepsin P) and zinc finger protein 831 (*Zfp831*) were significantly induced in the lungs of genetically heterogeneous Diversity Outbred (DO) mice exhibiting progressive TB, characterized by elevated pulmonary *Mtb* burden and inflammation [52]. In rhesus macaques, animals with progressive TB disease produced significantly more *CTSZ* and *ZNF831* (a high-confidence ortholog of *Zfp831*) transcript in their lungs [52]. In the blood of patients with active TB, *CTSZ* transcription was significantly elevated while *ZNF831*
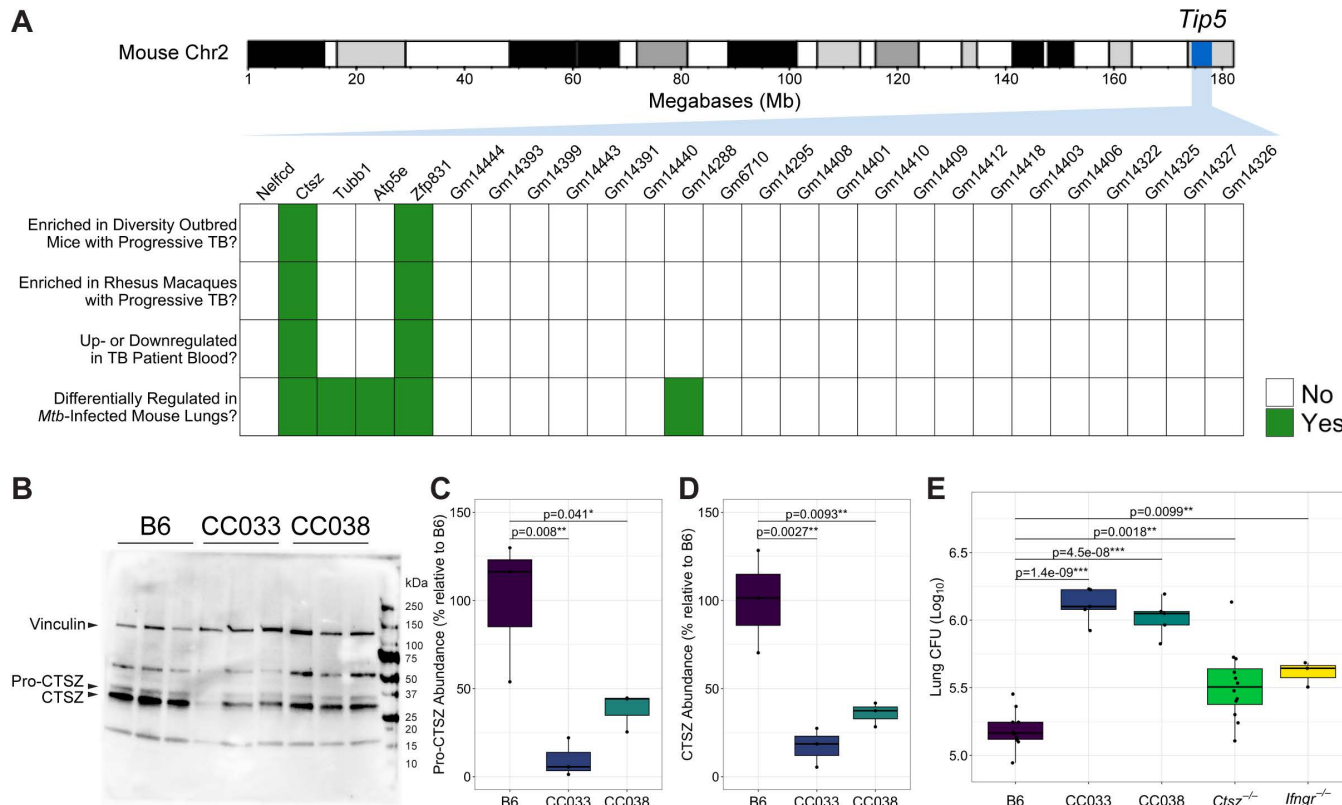
Fig 1. Identification and validation of *Ctsz* as the lead candidate gene underlying *Tip5*. (A) Heatmap representation of the per-gene outcome of four distinct criteria for genes within the *Tip5* QTL (95% CI: 174.29–178.25Mb): (i) whether the gene transcript is significantly enriched in the lungs of genetically heterogeneous Diversity Outbred (DO) mice experiencing elevated burden and inflammation after *Mtb* infection [52], (ii) whether the gene transcript is significantly enriched in the lungs of rhesus macaques exhibiting clinical symptoms of severe TB disease [52], (iii) whether the gene is significantly up- or down-regulated in the blood of individuals with active TB [54], and (iv) whether the gene is differentially expressed in inbred mouse lungs across variable host genotypes, *Mtb* strains, and infectious doses [53]. To be included in the heatmap, genes were required to encode proteins and to contain a known SNP from the NOD inbred line [55]. Mouse chromosome 2 image generated in the R package karyoploteR. **(B)** CTSZ protein was measured from the lung homogenate of uninfected B6 and the *Tip5^S* CC strains CC033 and CC038 ($n = 3$ mice per genotype). Each lane is a separate biological replicate. Vinculin served as the loading control. The assayed proteins are indicated by black arrows. Relative abundance of the **(C)** pro-CTSZ and **(D)** mature CTSZ protein between B6 and the *Tip5^S* CC strains, quantified from Fig 1B by normalizing CTSZ levels for each biological replicate to its respective vinculin level. Values plotted as a percentage of the mean CTSZ to vinculin band intensity ratio relative to the average ratio for B6 mice. Hypothesis testing was performed by one-way ANOVA and Dunnett's *post hoc* test on individual ratios between CTSZ and vinculin band intensities by genotype. **(E)** Bacterial burden measured from lung homogenate 4 weeks after aerosol infection with *Mtb* H37Rv ($n = 3$–12 mice per strain; all males except B6 and *Ctsz^{−/−}* groups, which included both sexes in equal proportion). Hypothesis testing was performed by one-way ANOVA and Dunnett's *post hoc* test on $\log_{10}$-transformed values. The data underlying this figure can be found in S1 Data sheets 1C, 1D, and 1E.

https://doi.org/10.1371/journal.pbio.3003377.g001

transcription was significantly repressed [52,54]. In an additional lung transcriptomic study in inbred mice leveraging distinct *Mtb* strains and infectious doses, only 5 gene transcripts within *Tip5*, including *Ctsz*, were differentially regulated across all strains and doses [53]. Currently, there is no established association between human *ZNF831* SNPs and TB outcomes. Conversely, mutations in human *CTSZ* were previously associated with poorer TB outcomes [23,24,26]. From this analysis, *Ctsz* was identified as a lead candidate for further interrogation as a potential genetic cause of *Tip5*-linked TB susceptibility.

The susceptible NOD variant of *Tip5* and ablation of *Ctsz* both impart TB susceptibility

To evaluate *Ctsz* as a causal factor underlying *Tip5*-linked susceptibility, we measured CTSZ protein from the lungs of uninfected CC strains harboring the susceptible NOD *Tip5* variant (CC033, CC038). Compared to *Mtb*-resistant B6, the

lungs of both CC033 and CC038 exhibited significantly lower baseline levels of CTSZ protein (Fig 1B), both in the pro-form (Fig 1C) and mature active form (Fig 1D). Collectively, these data suggest that the NOD *Tip5* haplotype contains a hypomorphic variant of *Ctsz*, resulting in reduced production of CTSZ protein in *Tip5^S* CC strains.

Considering the *Tip5* QTL was first identified in a large-scale in vivo screen, we next assessed whether *Tip5^S* CC strains and *Ctsz* null mice (*Ctsz$^{-/-}$*) (S1A Fig) are susceptible to aerosol infection, the natural route of *Mtb* infection. A cohort including B6, CC033, CC038, *Ctsz$^{-/-}$*, and highly susceptible interferon gamma receptor null mice (*Ifngr$^{-/-}$*) [56] was infected via aerosol route with *Mtb* H37Rv. The experiment terminated at 4 weeks postinfection, after the onset of adaptive immunity [57] and matching the initial CC screen endpoint [50]. Relative to B6, all infected strains exhibited significantly higher pulmonary *Mtb* burden (Fig 1E). The CC strains exhibited 10-fold greater lung CFU than B6, surpassing the canonically susceptible *Ifngr$^{-/-}$* mice. *Ctsz$^{-/-}$* mice exhibited a 2-fold increase in lung burden relative to B6. No significant differences were identified in disseminated spleen burden at this time point (S1B Fig). We conclude that *Tip5^S* CC strains and *Ctsz$^{-/-}$* mice exhibit reduced pulmonary bacterial control at 4 weeks postinfection.

Ctsz mediates lung CXCL1 levels early during *Mtb* infection

To characterize the impact of *Ctsz* on disease progression, we infected B6 and *Ctsz$^{-/-}$* mice via aerosol, sacrificing cohorts of mice at 2, 3, 4, and 8 weeks postinfection to capture innate and adaptive immune responses. *Ctsz$^{-/-}$* mice exhibited higher lung burden at 2 weeks (4.09 $\log_{10}$ CFU versus 3.41 in B6; $p < 0.05$) and 4 weeks (5.17 $\log_{10}$ CFU versus 4.09 in B6; $p < 0.05$) postinfection (Fig 2A). Similarly, at 3 weeks postinfection, *Ctsz$^{-/-}$* mice exhibited trends toward elevated spleen burden (2.68 $\log_{10}$ CFU versus 2.17 in B6; $p = 0.058$), suggesting earlier dissemination and weaker bacterial containment in the lungs of *Ctsz$^{-/-}$* mice (Fig 2B). However, by 4 weeks postinfection, spleen burden was indifferentiable between *Ctsz$^{-/-}$* and B6.

To profile the impact of *Ctsz* disturbance on the lung inflammatory response throughout the course of infection, we compared cytokine signatures of *Ctsz$^{-/-}$* with B6 at assayed timepoints. At 4 weeks postinfection, *Ctsz$^{-/-}$* mice exhibited higher concentrations of T_H1-associated cytokines, like TNF-α ($p = 0.019$) and IL-1β ($p = 0.016$), and lower levels of GM-CSF ($p = 3.8e^{-06}$), IL-6 ($p = 5.9e^{-04}$), LIF ($p = 6.6e^{-07}$), and VEGF ($p = 6.6e^{-07}$) compared to B6 (Fig 2C).

To identify unique features in the inflammatory signature of *Ctsz$^{-/-}$* mice, we performed sparse partial least squares discriminant analysis (sPLS-DA) across measured phenotypes (Fig 2D). Higher lung burden and CXCL1 levels in *Ctsz$^{-/-}$* mice were the strongest features underlying sparse component 1 (Fig 2E). Although component 1 explains 19% of variance in the data compared to 23% variance explained by component 2 (S2A Fig), component 1 better captures the variance attributable to genotype. CXCL1 has previously been identified as a biomarker of active TB disease in genetically diverse mice [51] and in humans [58]. From 2 to 4 weeks postinfection, *Ctsz$^{-/-}$* mice exhibited significantly higher lung CXCL1 levels (Fig 2F), suggesting that *Ctsz* ablation increases disease severity. However, by 8 weeks postinfection, although mean CXCL1 levels in *Ctsz$^{-/-}$* lungs were elevated, the difference was no longer significant. Enhanced production of CXCL1 was consistent throughout infection, suggesting that this effect may occur independent of differences in *Mtb* burden.

To explore the possibility that elevated CXCL1 levels may occur independent of infection in *Ctsz$^{-/-}$* mice, we sacrificed uninfected mice of both sexes. From lung homogenate, we found elevated levels of CXCL1 in *Ctsz$^{-/-}$* compared to B6 (Fig 2C; $p = 0.007$), suggesting that the connection between *Ctsz* and CXCL1 extends beyond the context of infection. Notably, the total CXCL1 levels in uninfected mice were comparable to levels measured at 2 weeks postinfection.

To determine whether *Ctsz* ablation alone is sufficient to confer susceptibility to aerosolized *Mtb* H37Rv, we conducted two longitudinal challenges of B6 and *Ctsz$^{-/-}$* mice in which mice were sacrificed when IACUC-approved humane endpoints were reached. *Ctsz* ablation was associated with a significant reduction in survival time (Fig 2G), which was driven by male mice (S2B and S2C Fig). Thus, disease progression in a host lacking *Ctsz* is characterized by increased lung *Mtb* burden, elevated lung CXCL1 levels indicative of heightened inflammation, and overall mortality risk.
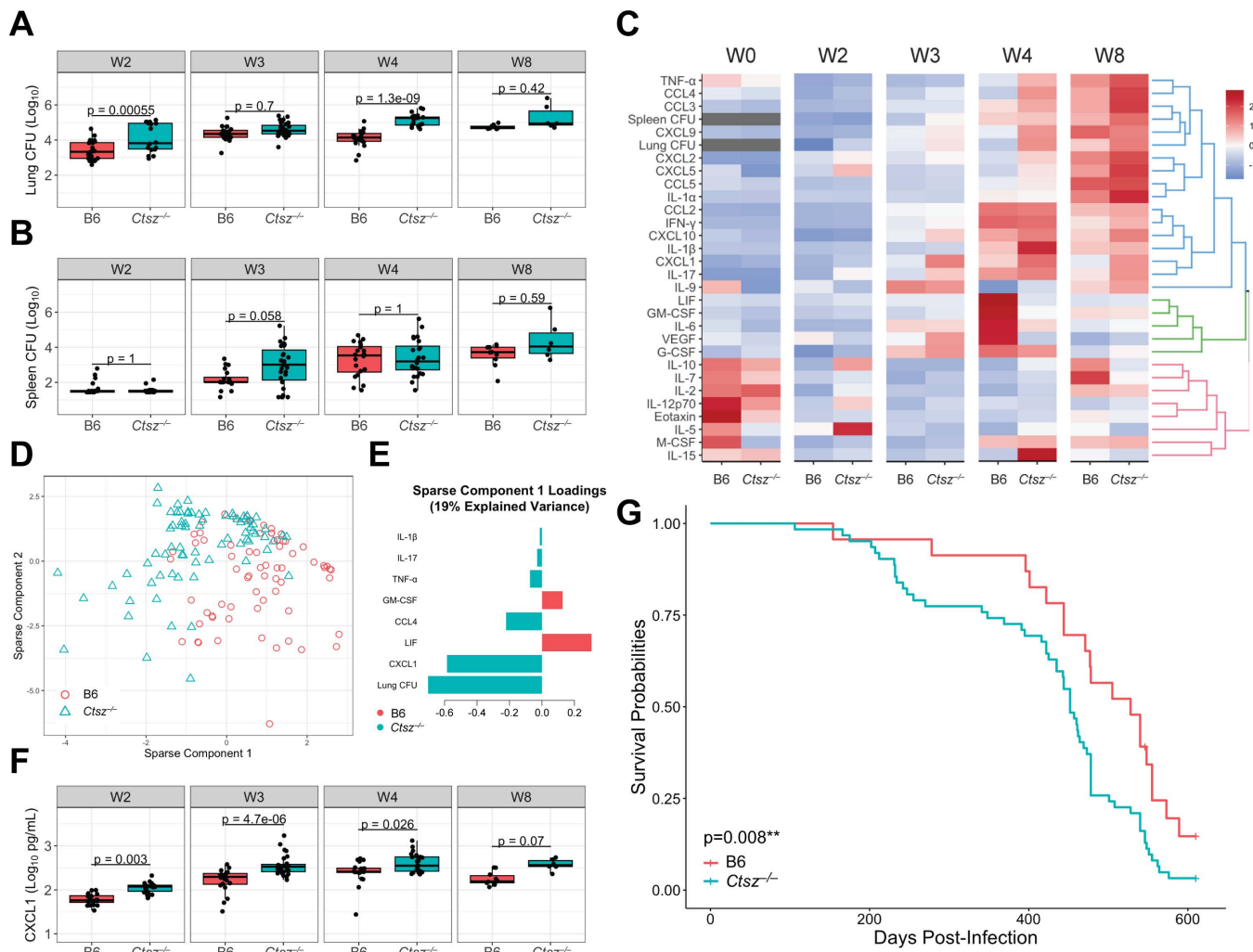
Fig 2. *Ctsz*^−/−^ mice have higher lung burden and earlier spleen dissemination during acute infection followed by greater chronic inflammation and mortality risk. *Mtb* burden measured from **(A)** lung and **(B)** spleen homogenate by dilution plating. **(C)** Heatmap depicting scaled and centered phenotypes, hierarchically clustered and separated into 3 k clusters. **(D)** Individual mice plotted against the first two sPLS-DA components, which explained the greatest variance in the data after optimization. **(E)** Phenotype loadings contributing to component 1. Component 2 loadings shown in S2A Fig. **(F)** CXCL1 levels measured from lung homogenate by multiplex ELISA. For panels A, B, and F, hypothesis testing was performed by two-way ANOVA and Tukey's *post hoc* test on $\log_{10}$-transformed values. For panels A–F, mice were sacrificed at 2, 3, 4, and 8 weeks following aerosolized *Mtb* H37Rv infection. Data are from two independent experiments with $n = 6$–14 mice per genotype, representative of both sexes, at each time point. In panel C, age-matched, uninfected mice ($n = 3$–4 per genotype and sex) were assayed for comparison (designated "W0"). **(G)** Kaplan–Meier survival estimates of aerosol-infected B6 ($n = 23$) and *Ctsz*^−/−^ mice ($n = 62$) across two independent experiments. Hypothesis testing was performed using a log-rank test. Equal proportions of both sexes were included. Mice that were not moribund at time of sacrifice were censored for analysis. The data underlying this figure can be found in S1 Data sheets 2ABCDEF_S2A and 2G_S2BC.

https://doi.org/10.1371/journal.pbio.3003377.g002

Disturbance of *Ctsz* enhances CXCL1 induction in macrophages

To explore the expression of cathepsin Z across species and mycobacterial infection models, we analyzed two previously published single-cell RNA sequencing (scRNA-Seq) datasets. In zebrafish infected with *Mycobacterium marinum (Mm)*, *ctsz* was most highly expressed in inflammatory macrophages (cluster 9) after 14 days of infection (Fig 3A–3C) [59]. *CTSZ* in cynomolgus macaques was most highly expressed in macrophages 4 weeks after *Mtb* infection compared to other assayed cell types (Fig 3D–3F) [60]. These results agree with literature establishing the presence of CTSZ in
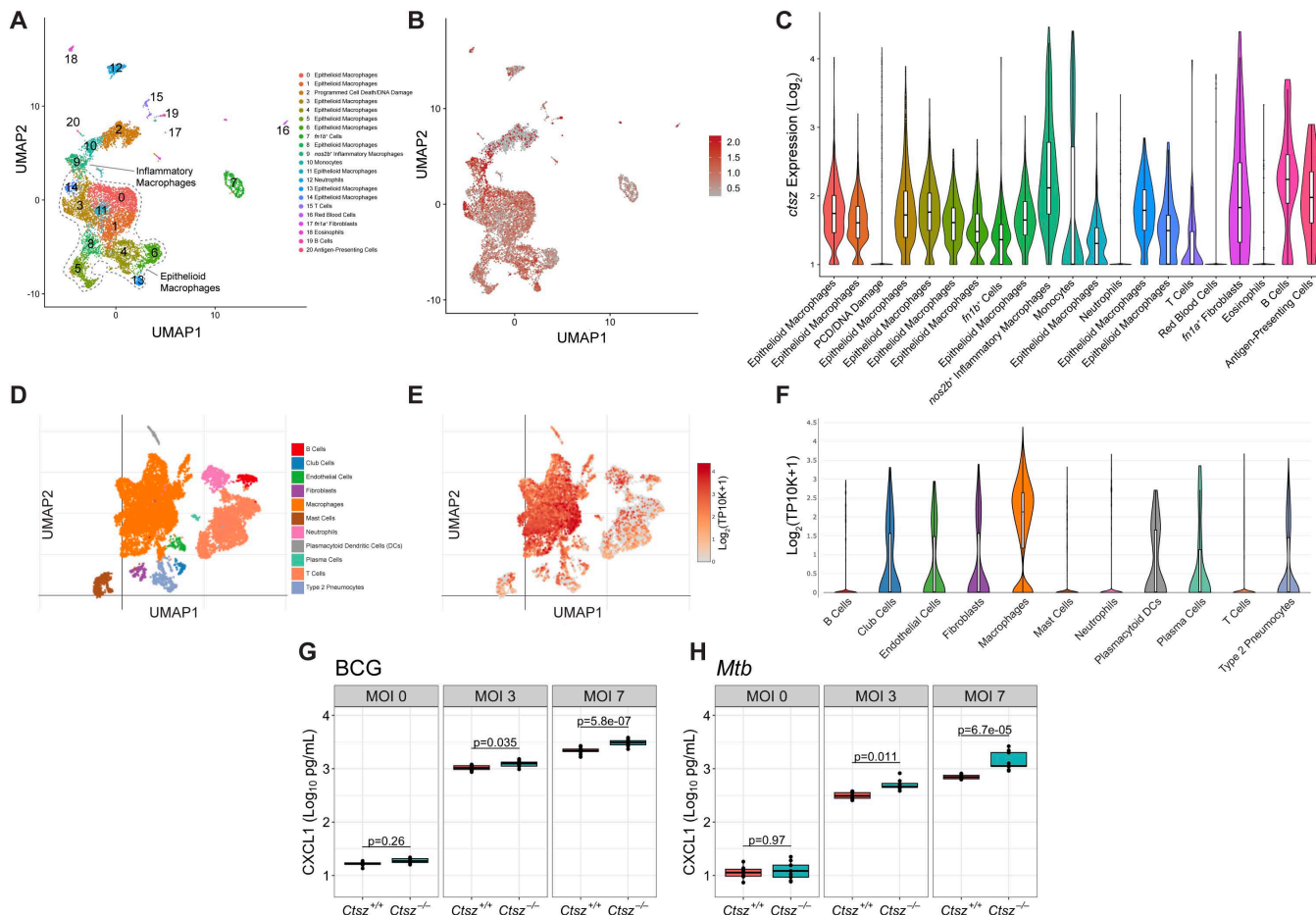
Fig 3. Cathepsin Z is highly expressed in macrophages across species following mycobacterial infection and mediates levels of CXCL1 in murine macrophages. (A) UMAP showing scRNA-Seq results from zebrafish granulomas infected with *M. marinum* (*Mm*), generated by reanalysis of previously published data from by Cronan and colleagues [59]. Cells are colored by cluster and assigned in an unsupervised approach from transcriptional signatures. Clusters were annotated by the authors. **(B)** ScRNA-Seq data colored by relative expression of zebrafish *ctsz* in *Mm*-infected granulomas, with highest expression levels observed in cluster 9. **(C)** Violin plots depicting the relative *ctsz* expression by cell cluster, with fill colors and cluster labels aligned with panel **A**. **(D)** UMAP showing scRNA-Seq of granulomas extracted from *Mtb*-infected cynomolgus macaques at 4 weeks postinfection, published by Gideon and colleagues, 2022 [60]. Data accessed at the Broad Institute Single Cell online repository on October 3, 2023 (https://singlecell.broadinstitute.org/single_cell/study/SCP1749/). **(E)** ScRNA-Seq data colored by relative expression of *CTSZ* in *Mtb*-infected macaque granulomas. **(F)** Violin plots depicting the relative *CTSZ* expression by cell type, with fill colors and cell type labels aligned with panel D. CXCL1 levels measured in triplicate at 24 h postinfection from **(G)** BCG-infected and **(H)** *Mtb*-infected BMDMs by ELISA. For panels G and H, BMDMs were differentiated from independent pairs of *Ctsz*⁺/⁺ and *Ctsz*⁻/⁻ sibling males for each infection (*N*=3 infections per pathogen). Dashed threshold denotes the limit of detection for the ELISA. Statistical significance was determined by two-way ANOVA and Tukey's *post hoc* test on batch-corrected, log₁₀-transformed values. The data underlying this figure can be found in S1 Data sheets 3G and 3H. Data from Cronan and colleagues (2021) and Gideon and colleagues (2022) are available in the NCBI Gene Expression Omnibus (GEO) under accession numbers GSE161712 and GSE200151, respectively.

https://doi.org/10.1371/journal.pbio.3003377.g003

monocytes and macrophages [27–30] and further highlight that cathepsin Z expression in these cell types following mycobacterial infection is conserved across diverse host species.

As cathepsin Z is consistently expressed in macrophages across several species following mycobacterial infection, we sought to characterize the impact of *Ctsz* ablation on the initial macrophage response to mycobacterial exposure. To test if macrophages contribute to the increased production of CXCL1 during infection in *Ctsz*⁻/⁻ mice, we generated BMDMs from *Ctsz*⁺/⁺ and *Ctsz*⁻/⁻ sibling pairs. When infected with either nonpathogenic *Mycobacterium bovis* (Bacillus Calmette-Guérin;

BCG) (Fig 3G) or Mtb (Fig 3H), *Ctsz*$^{-/-}$ macrophages produced greater amounts of CXCL1 than *Ctsz*$^{+/+}$ by 24 h postinfection. In both infection models, this effect scaled with increasing multiplicity of infection (MOI). Thus, the elevated CXCL1 we observed in *Ctsz*$^{-/-}$ lungs may be driven by macrophages, especially during the early stages of infection, and appears to be independent of mycobacterial pathogenicity. These results from *Mtb*-infected *Ctsz*$^{-/-}$ mice and BMDMs suggest an interaction between CTSZ and CXCL1 following bacterial exposure.

Variants in human *CTSZ* are associated with TB severity

To investigate the impact of natural *CTSZ* variation on human TB disease outcomes, we examined whether human *CTSZ* variants are associated with TB disease severity in a household contact study in Uganda ($n = 328$ across two independent cohorts) [61]. Of 81 observed *CTSZ* SNPs, 20 SNPs were associated with differences in Bandim TBScore, a TB severity index (S1 Table; unadjusted $p < 0.05$, linear model with sex, HIV status, and genotypic principal components 1 and 2 as covariates) [62]. After performing a Bonferroni adjustment for multiple comparisons, 4 SNPs and 1 INDEL maintained associations with TB disease severity (Table 1). These variants are in strong linkage disequilibrium (LD) with one another ($R^2 > 0.8$), suggesting that they represent a single haplotype block (Fig 4A). For the most significant SNP (rs113592645), the minor T allele is associated with decreased TB disease severity between those with homozygous major C allele and heterozygotes (Fig 4B, results for other haplotype SNPs included in S3A–3C Fig). To investigate the potential impact of the TB severity SNPs on *CTSZ* expression, we used published RNA-Seq data [63] to compare *CTSZ* transcript levels across *Mtb*- and mock-infected monocytes between genotypes at each *CTSZ* SNP. In the cohort of human-derived monocytes, *CTSZ* was highly expressed at baseline and was downregulated following *Mtb* infection (Fig 4C). Conversely, the rs113592645 minor T allele was associated with increased *CTSZ* expression following *Mtb* infection ($p = 0.0395$; Fig 4D; other haplotype SNP results in S3D–3F Fig). This effect was not observed following mock infection conditions ($p = 0.108$; Fig 4D). Together, these data suggest that these *CTSZ* variants are associated with both TB disease severity and divergent transcription of *CTSZ* following *Mtb* infection.

CTSZ is produced in macrophages associated with human pulmonary granulomas

The mycobacterial granuloma is an organized structure that can develop within human hosts to contain and restrict *Mtb* infection and is composed of heterogeneous immune cell populations, predominantly macrophages [66]. To investigate whether *CTSZ* expression in macrophages is conserved between mice and humans, we reanalyzed published, spatially resolved scRNA-Seq data from human *Mtb* granulomas [65]. In pulmonary granulomas biopsied from three patients with TB, *CTSZ* was highly upregulated in macrophage cell clusters (Fig 4E–4G). Within patient-derived pulmonary granuloma sections, areas of elevated *CTSZ* expression were found to coincide with regions dominated by macrophages (Fig 4H).

Table 1. *CTSZ* SNPs significantly associated with TB severity in Ugandan household contact study cohorts, sorted by ascending *p*-value. Included SNPs were significantly associated with Bandim TBScore after Bonferroni correction for multiple comparisons ($p < 0.05$). Complete collection of 81 SNPs can be found in S1 Table. SNPs are annotated as described in McHenry and colleagues [61]. Allele effects were assessed using a linear mixed effect model in the R package kimma to account for sex, HIV status, and genotypic principal components 1 and 2. Cohorts 1 and 2 are independent cohorts of culture-confirmed adult TB cases. Abbreviations: SNP, single-nucleotide polymorphism; CHR, chromosome; BP, base pair from GRCh38 build; Adj., adjusted; MAF, minor allele frequency.

| SNP	CHR:BP	Effect Allele	Adj. p-value	β	MAF in Cohort 1 (n = 149)	MAF in Cohort 2 (n = 179)
rs113592645	20:59001340	T	0.0001814	−1.0036	0.18	0.061
rs111630627	20:59002589	G	0.0003077	−0.9268	0.18	0.075
rs138964736	20:59002671	ACTTTG	0.0003077	−0.9268	0.18	0.075
rs76687632	20:59002905	G	0.0003077	−0.9268	0.18	0.075
rs8120779	20:59001977	G	0.0003942	−0.8671	0.18	0.095

https://doi.org/10.1371/journal.pbio.3003377.t001
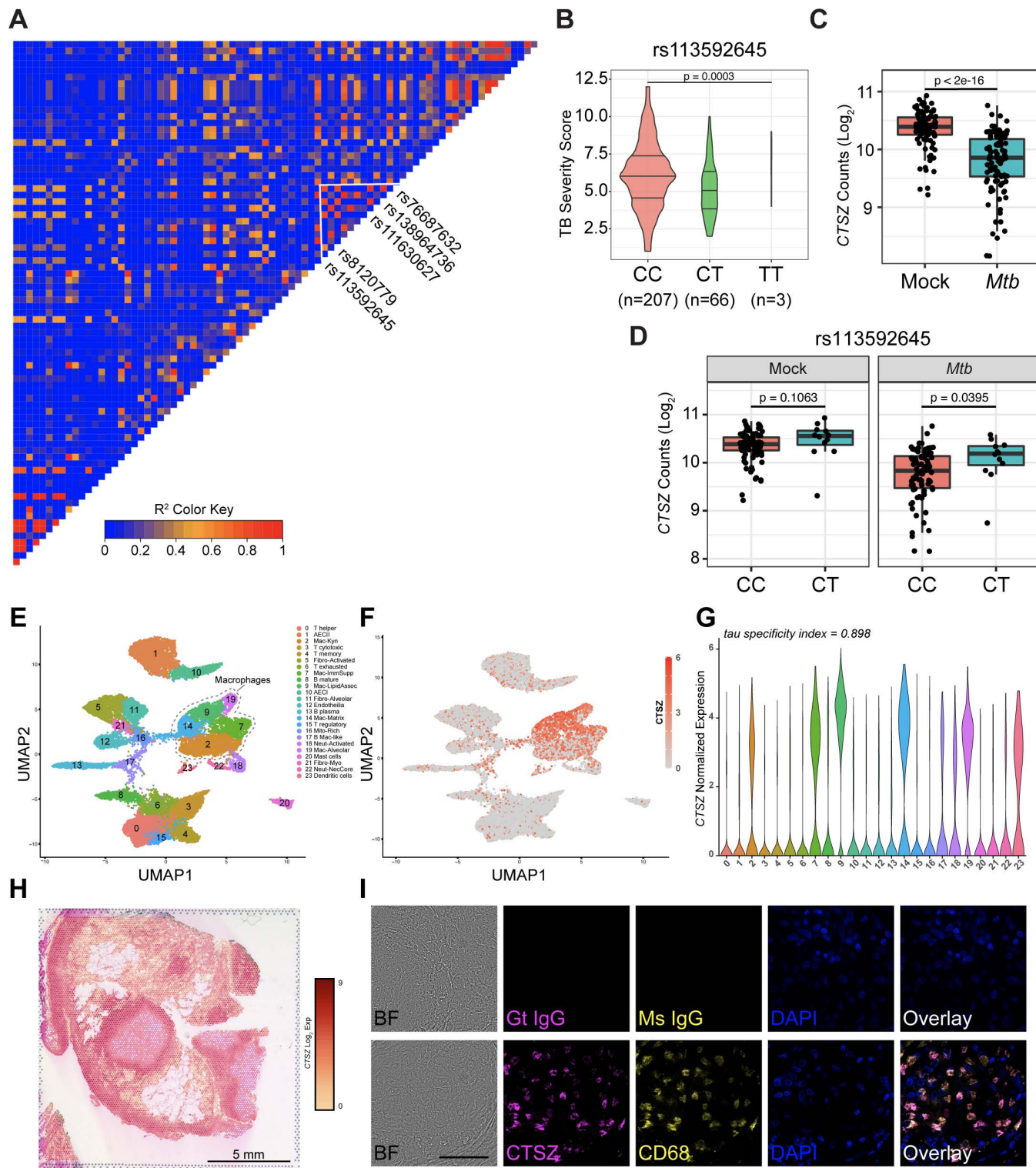
Fig 4. Human *CTSZ* variants are associated with TB severity, and CTSZ is present at the host-pathogen interface within human pulmonary *Mtb* granulomas. (A) LD plot of human *CTSZ*, highlighting a haplotype block of 4 identified SNPs and 1 INDEL associated with TB disease severity. **(B)** Comparison of TB severity, measured using Bandim TBScore, by genotype for the lead TB severity SNP, rs113592645. TB severity score by genotype for remaining SNPs can be found in S3A–3C Fig. For panels C and D, *CTSZ* expression was profiled by RNA-Seq in monocytes from 100 Ugandan

individuals. Human-derived monocytes were subjected to 6-hour *Mtb* and mock infection conditions. **(C)** Counts of *CTSZ* transcript ($\log_2$ counts per million) collected following mock and *Mtb* infection. **(D)** Counts of *CTSZ* transcript ($\log_2$ counts per million) according to genotype for the lead TB severity SNP, rs113592645, following mock and *Mtb* infection. Measurements for homozygous minor allele (TT) were excluded due to low sample size. Counts of *CTSZ* transcript by genotype of remaining SNPs can be found in S3D–3F Fig. **(E)** A manually annotated UMAP generated by unsupervised clustering of data from single-cell mRNA-Seq of human biopsy tissue, containing *Mtb* granulomas from three patients with TB. **(F, G)** Analysis of normalized expression values reveals that *CTSZ* is specifically induced in granuloma macrophages, particularly in lipid-associated macrophages. Values of tau near 1 indicate that *CTSZ* expression is highly specific to some clusters, whereas values near 0 indicate uniform expression across clusters [64]. This expression pattern is part of a broader induction of multiple cathepsins in human *Mtb* granuloma macrophages, shown in S4A Fig. **(H)** The positional distribution of *CTSZ* expression in human *Mtb* granulomas as determined by Visium v2 spatial mRNA-Seq of Eosin-stained biopsy tissue sections from a patient with TB. Similarly processed pulmonary and pleural biopsies from two additional patients with TB can be found in S4B Fig. Panels E–H were generated by reanalysis of data from Pyle and colleagues, 2025 [65]. Cell clusters were annotated by the authors. **(I)** Brightfield (BF) images and immunofluorescent staining of CTSZ and CD68 within a granuloma biopsy from an individual with pulmonary TB. Goat (Gt) and mouse (Ms) IgG isotype control staining is depicted in the top row. DAPI staining indicates cell nuclei. Scale bar is 60 μM in length. Images were captured at 100× magnification. The data underlying this figure can be found in S1 Data sheet 4CD_S3DEF. Data from Pyle and colleagues (2025) are available in the NCBI GEO under accession numbers GSE296399 and GSE296400.

https://doi.org/10.1371/journal.pbio.3003377.g004

In addition to *CTSZ*, several other cathepsins were also found to be induced in human *Mtb* granuloma macrophages (S4 Fig). To confirm whether elevated *CTSZ* transcription corresponded with elevated CTSZ protein levels in patient tissue samples, we performed immunostaining on granulomas biopsied from the lungs of patients with culture-confirmed TB. We positively identified CTSZ within granuloma-associated CD68+ macrophages from *Mtb*-infected lung tissue (Fig 4I). Thus, CTSZ is produced at the site of host-pathogen interaction in humans, suggesting that native functions at this interface could be interrupted should CTSZ production or localization be impeded. Combined with the results from *Ctsz* null mice, these data suggest that balancing cathepsin Z levels is required to regulate lung inflammation and reduce risk of mortality following *Mtb* infection. Collectively, these data establish an association between human *CTSZ* variants and TB disease severity and reveal CTSZ as a granuloma macrophage-associated protein in human lungs.

Discussion

Over 15 years have passed since the initial discovery that human *CTSZ* is linked with TB disease susceptibility in West and South Africa. However, the relationship between *Mtb* susceptibility and CTSZ had yet to be experimentally determined. We show that genetic interruption of *Ctsz* in mice causes a failure of bacterial restriction and overproduction of CXCL1 during early *Mtb* infection, precipitating an increased risk of mortality. We further show that ablation of *Ctsz* is associated with cell-autonomous overproduction of CXCL1 in macrophages following *Mtb* infection. We report 4 SNPs and 1 INDEL within *CTSZ* significantly associated with TB severity in Ugandan individuals and show elevated *CTSZ* expression in infected monocytes from this cohort. Finally, we find that CTSZ protein is produced within the CD68+ macrophages in human granulomas, the pulmonary structure that contains and restricts *Mtb* growth.

CTSZ participates in several known immunological pathways [29,32,33,67]. For example, CTSZ is known to interact with cell surface integrins that mediate immune cell activity, including lymphocyte function-associated antigen-1 (LFA-1) [32,33] and macrophage-1 antigen (Mac-1) [67], which regulates *Mtb* phagocytosis [68] and phagocyte migration. Here, we show that lung CXCL1 levels are consistently elevated in *Ctsz*−/− mice prior to and throughout infection. Moreover, compared to wildtype siblings, *Ctsz*−/− macrophages produce more CXCL1 in response to pathogenic and nonpathogenic mycobacterial infection, suggesting a broad immunological response to bacterial exposure.

CXCL1, a cytokine associated with severe TB disease in mice [51] and in humans [58], is primarily known as a neutrophil chemoattractant [69]. Both *Ctsz* and *Cxcl1* are induced in *Mtb*-infected mice [70]. We are not the first to show a significant increase in CXCL1 levels following pathogenic infection in *Ctsz*−/− mice [71], but to the best of our knowledge, this is the first study to directly link CTSZ and CXCL1 during TB pathogenesis. In a 2022 study, mice with neutrophil-specific ablation of the Mac-1 subunit integrin β_2 (CD18) were infected with *Aspergillus fumigatus*, a fungus that is recognized by the immune system through Mac-1 [72]. By 24 h postinfection, Haist and colleagues observed elevated fungal

burden and elevated CXCL1 levels in bronchoalveolar lavage fluid. Similarly, we have observed high *Mtb* burden and CXCL1 in *Ctsz*⁻/⁻ lungs following *Mtb* infection. These results collectively suggest that disturbance of normal CD18 activity, which is known to rely upon *Ctsz* [32,33,67,73,74], may trigger overproduction of CXCL1. Future studies are needed to delineate the implications of this CTSZ-CXCL1 axis with other known roles of CTSZ, including cellular adhesion, migration, and antigen presentation [29].

A deeper understanding of how the functions of CTSZ impact disease severity could prove vital to developing therapeutic strategies for both endogenous and infectious diseases. Men are 1.7-fold more likely to develop active TB than women [75]. Considering the sexually dimorphic mortality risk observed in *Ctsz*⁻/⁻ mice and a previous study reporting that B6 BMDM inflammatory responses are divergent between sexes [76], further study of the sex-specific effects of CTSZ may yield insights into the biology underpinning this imbalance in humans. Beyond TB, CTSZ has been implicated as a mediator of host response during *Helicobacter pylori* infections of patient-derived monocytes and *Salmonella* Typhimurium infections of murine BMDMs [77,78]. Furthermore, mouse and human studies have investigated CTSZ for roles in aging [79,80] and in a number of endogenous conditions, including multiple sclerosis [81], primary biliary cholangitis [82,83], osteoporosis [84], and Alzheimer's [85]. *CTSZ* has also been explored for prognostic value and roles in tumor progression across many cancers [86], including breast [87], colorectal [88], gastric [77], and prostate cancers [89], and hepatocellular carcinoma [90]. Increased *CTSZ* expression was associated with poor patient prognoses in two studies [88,90], with one study proposing *CTSZ* as a putative oncogene [90]. Given the importance of CTSZ across a spectrum of human disease categories, continued study of *CTSZ* may yield insights on the human response to departures from immune homeostasis.

While much remains unknown about the molecular roles of CTSZ during *Mtb* infection, this study is the first, to our knowledge, to identify cathepsin Z as a molecular determinant of TB severity in mice and humans. This study is also the first to report CTSZ localization within granuloma-associated CD68⁺ macrophages in *Mtb*-infected human lungs. Host genetic diversity is a central predictor of TB severity, and consideration of genetic diversity is essential to combat human pathogens as enduring and prolific as *Mtb*.

Materials and methods

Ethics statement

All animal studies were conducted in accordance with the guidelines issued in the Guide for the Care and Use of Laboratory Animals of the National Institutes of Health and the Office of Laboratory Animal Welfare. Mouse studies were conducted at Duke University using protocols approved by the Duke Institutional Animal Care and Use Committee (IACUC) (Animal Welfare Assurance #A221-20-11 and #A204-23-10) in a manner designed to minimize pain and suffering in *Mtb*-infected animals. Any animal exhibiting signs of severe disease was immediately euthanized in accordance with IACUC-approved endpoints. Use of patient samples was approved by the Duke University Medical Center Institutional Review Board (IRB) under Protocol #00107795 and the University of Washington IRB under Protocol STUDY00001537. Patient sample processing at Duke University was carried out by Drs. Jadee Neff, Charlie Pyle, and Jason Stout. The human genetic data were obtained from the Kawempe Community Health Study in Uganda, which was approved by the National HIV/AIDS Research Committee of Makerere University (Protocol #014) and the University Hospitals Cleveland Medical Center IRB (Protocol #10-01-25). Final clearance was given by the Uganda National Council for Science and Technology (Ref #658).

Mice

Male and female C57BL/6J (#000664) and male B6.129S7-*Ifngr1*^tm1Agt^/J (*Ifngr*⁻/⁻; #003288) mice were purchased from The Jackson Laboratory. Male CC033/GeniUncJ (CC033) and CC038/GeniUnc (CC038) mice were purchased from the University of North Carolina (UNC) Systems Genetics Core Facility (SGCF). *Ctsz*⁻/⁻ mice were generously provided by Robin Yates (University of Calgary, Calgary, AB, Canada) and generated as previously described [91]. *Ctsz*⁺/⁺ and *Ctsz*⁻/⁻ mice

were subsequently bred at Duke, using *Ctsz*⁺/⁻ breeding pairs to enable generation of sex-matched *Ctsz*⁺/⁺ and *Ctsz*⁻/⁻ siblings. All mice were housed in a specific pathogen-free facility within standardized living conditions (12-h light/dark, food, and water *ad libitum*). Aerosol-infected mice were matched at 8–12 weeks of age at the time of *Mtb* infection. Mice were individually identified for weighing and wellness assessment throughout infection using Bio Medic Data Systems implantable electronic ID transponders (TP-1000) implanted subcutaneously at the back of the neck prior to infection.

Genotyping

In-house confirmation of *Ctsz*⁻/⁻ genotype was performed using forward primer 5′-TTG CTG TTG GCG AGT GCG-3′ and reverse primer 5′-CTT GTC ACC AGA TTC CAG C-3′ to detect wildtype *Ctsz* and forward primer 5′-GCT ACC TGC CCA TTC GAC-3′ and reverse primer 5′-ACA GTA GGA CTG GCC AGC-3′ to detect knockout product. Primer sequences were generously provided by Robin Yates (University of Calgary, Calgary, AB, Canada). DNA was extracted from tissue samples using the DNEasy Blood & Tissue Kit (Qiagen). DNA products were prepared for PCR using Q5 High-Fidelity Master Mix (New England BioLabs) and amplified. Protocol included initial 98 °C (30s), then 34 cycles of denaturation (98 °C, 10s), annealing (68 °C, 30s), and extension (72 °C, 90s), and a final 72 °C (180s), resting at 10 °C ∞ until stopped. Amplified products were separated on a 1% agarose-TAE gel using SYBR Safe stain (Thermo Fisher Scientific) and 1kb Plus DNA Ladder (New England BioLabs). *Ctsz*⁺/⁺ and *Ctsz*⁻/⁻ mice were genotyped at the time of weaning from ear and tail tissue biopsies by TransnetYX (Cordova, TN, USA) using proprietary RT-PCR primers designed to detect both *lacZ*, present in the IRES vector disturbing the second exon of *Ctsz* [91], and wildtype *Ctsz*.

Bacterial strains and culture

All infections were performed with either *Mtb* H37Rv genotype or *M. bovis* BCG (Bacillus Calmette-Guérin) Danish (gift from Sunhee Lee, University of Texas Medical Branch, Galveston, TX, USA), which was transformed with pTEC-15 wasabi fluor and possesses a hygromycin resistance marker for selection [92]. Aerosol infections were performed using an *Mtb* H37Rv strain confirmed to be positive for the cell wall lipid and virulence factor phthiocerol dimycocerosate (PDIM; gift from Kyu Y. Rhee, Weill Cornell Medicine, New York, NY, USA). Bacteria were cultured in Middlebrook 7H9 medium supplemented with oleic acid-albumin-dextrose catalase (OADC), 0.2% glycerol, and 0.05% Tween 80 (or 0.005% tyloxapol for macrophage infections) to log-phase with shaking (200rpm) at 37 °C. Hygromycin (50μg/mL) was added when necessary. Prior to all in vivo infections, cultures were washed and resuspended in phosphate-buffered saline (PBS) containing 0.05% Tween 80 (hereafter PBS-T). Bacterial aggregates were then broken into single cells using a blunt needle before diluting to desired concentration for infection.

Mouse infections

Mice were infected with ~150−350 *Mtb* CFU via aerosol inhalation (Glas-Col). On the day following each infection, one cage was sacrificed to enumerate lung CFU as an approximation of infectious dose. For all infections, mice were euthanized in accordance with approved IACUC protocols, and lung and spleen were harvested into PBS-T and processed in a FastPrep-24 Homogenizer (MP Biomedicals, 4.0 m/s, 45s, 2–3×). *Mtb* burden was quantified by dilution plating onto Middlebrook 7H10 agar supplemented with OADC, 0.2% glycerol, 50 μg/mL Carbenicillin, 10 μg/mL Amphotericin B, 25 μg/mL Polymyxin B, and 20 μg/mL Trimethoprim. Lung homogenate was centrifuged through a 0.2 μm filter to collect decontaminated filtrate, and cytokines and chemokines were assayed using the pro-inflammatory focused 32-plex assay (Eve Technologies, Calgary, AB, Canada).

Human tissue immunofluorescent staining

Patient tissue samples containing *Mtb* granulomas were identified at the Duke University School of Medicine. Clinical tissue specimens were obtained from the Duke Pathology Department, and 5 μm paraffin sections for antibody staining were

cut by the Research Histology Laboratory within the BioRepository & Precision Pathology Center (BRPC). Paraffin was dissolved using two xylene washes followed by washes with ethanol of increasing dilution (100% twice, 95% twice, 70% once, and 50% once), three washes with deionized water, and a final wash in PBS. Sample was placed in antigen retrieval buffer (10 mM Tris/1 mM EDTA, pH 9.0) and processed in a pressure cooker for 10 min. Following a cooling step, samples were blocked for an hour in 2.5% normal donkey serum. Samples were incubated overnight at 4 °C with Goat anti-Human/Mouse/Rat Cathepsin X/Z/P Polyclonal Antibody (R&D Systems, AF934, 0.185 mg/mL) and Mouse anti-Human CD68 Monoclonal Antibody (Agilent Dako, M081401-2, 0.185 mg/mL) in 2.5% serum in a humidified chamber. Immunoglobulin G (IgG) isotype controls for background staining (Goat: Biotechne, AB-108-C, 1 mg/mL stock; Mouse:GenScript, A01007, 1 mg/mL stock; Rabbit: Invitrogen, 10500C, 3 mg/mL provided) were also used. Primary antibody was removed with three washes of PBS and two of deionized water. Samples were incubated in Alexa Fluor (AF) conjugated secondary antibody (Thermo Fisher Scientific, 1:500; Donkey anti-Goat IgG AF Plus 647:A32849; Donkey anti-Mouse IgG AF 488:A-21202; Donkey anti-Rabbit IgG AF 555:A-31572) in 2.5% serum for 1–3 h. Following three PBS washes, the samples were mounted for imaging in DAPI Fluoromount-G (Southern Biotech, 0100-20) on glass slides (Fisher Scientific, 22-035813). All antibodies used for staining were centrifuged at 10,000 RCF (4 °C) for 10 min to remove antibody precipitate prior to use.

Microscopy analysis

Human samples were imaged at 100× on a Zeiss Axio Observer Z1 inverted microscope with an X-Light V2 spinning disk confocal imaging system (Biovision). Images were processed identically within Fiji software (v2.14.0/1.54f) for image clarity.

Bone marrow-derived macrophage infections

$Ctsz^{+/+}$ and $Ctsz^{-/-}$ sibling pairs were sacrificed in accordance with approved IACUC protocols between 10 and 12 weeks of age. For BCG infections, bone marrow was flushed from hip and leg bones with DMEM (Corning) and cultured for a week at 37 °C in a sterile solution of DMEM with 10% heat-inactivated fetal bovine serum (Corning), 18% 3T3-derived M-CSF, 1× Pen/Strep (Corning), and 25 mM HEPES (gibco). For Mtb infections, bone marrow was flushed from hip and leg bones with sterile DMEM (Corning) and frozen in 10% DMSO in heat-inactivated fetal bovine serum (Corning). Aliquots were later thawed and cultured for a week at 37 °C in a sterile solution of DMEM with 10% heat-inactivated fetal bovine serum (Corning), 30 µg/mL recombinant M-CSF (PeproTech), 1X Pen/Strep (Corning), and 25 mM HEPES (gibco). Differentiated macrophages were then plated at a concentration of $3 × 10^5$ cells/well in a 24-well plate and cultured at 37 °C overnight in a DMEM solution as above but without Pen/Strep. BMDMs were infected with BCG or transported to BSL-3 biocontainment for infection with Mtb at MOI 3 or 7 or left uninfected. Wells were tested for even infection by CFU plating. At 24 h postinfection, supernatants were collected and filtered using a 0.2 µm filter to remove bacteria. Cytokines and chemokines were assayed from using the high-sensitivity 18-plex discovery assay (Eve Technologies, Calgary, AB, Canada).

Western blotting

For the comparison of mouse CTSZ between uninfected B6 mice and $Tip5^s$ CC strains (CC033 and CC038), whole lungs were collected from male mice (8 weeks of age) into 1 mL of Trizol reagent. Samples were homogenized with sterile beads at 4.5 m/s for 30 s using the FastPrep-24 Homogenizer (MP Biomedicals). For samples in Trizol, protein was precipitated for 15 min using 9 volumes of 100% methanol at room temperature. The protein precipitate was centrifuged at 3,000 rpm for 5 min, dried for 5 min, and washed in an equal volume of 90% methanol. The protein precipitates were then centrifuged for 1 min at 3,000 rpm, dried for 10 min, resuspended in 1 mL of RIPA buffer and 1× Protease Inhibitor Cocktail, and heated for 5–10 min at 95 °C. Equal volumes of each sample were combined with Laemmli Sample Buffer (BioRad) and

2-Mercaptoethanol (BioRad) and heated at 95 °C for 5 min. SDS-PAGE was performed using BioRad Western Blotting kit along with Precision Plus Protein All Blue Prestained Protein Standards (BioRad). Protein was separated using a 4%–20% Mini-PROTEAN TGX Stain-Free Protein Gel (BioRad) and transferred to a polyvinylidene fluoride (PVDF) membrane using a semi-dry transfer protocol on a Trans-Blot Turbo Transfer System (BioRad). Membrane was blocked using EveryBlot Blocking Buffer (BioRad). Primary staining was performed at 4 °C overnight using Human/Mouse/Rat Cathepsin X/Z/P Antibody (R&D Systems; AF934; 1:2,000 dilution in EveryBlot Blocking Buffer). For B6 and $Tip5^S$ CC mice, 0.1% Tween 20 was added to the blocking buffer and primary staining also included Vinculin (E1E9V) XP Rabbit mAb (Cell Signaling; #13901; 1:5,000 dilution in EveryBlot Blocking Buffer + 0.1% Tween 20). For $Ctsz^{+/+}$ and $Ctsz^{-/-}$ mice, secondary staining was performed at room temperature for 60 min using Donkey anti-Goat 680 (LI-COR; 1:20,000 dilution in EveryBlot Blocking Buffer + 0.1% SDS). Blot was washed in TBS-T between blocking and antibody stains, and fluorescence was measured using a LI-COR Odyssey. Secondary staining for B6 and $Tip5^S$ CC mice was performed at room temperature for 60 min using HRP-conjugated Rabbit Anti-Goat IgG (Proteintech; SA00001-4; 1:5,000 dilution in EveryBlot Blocking Buffer + 0.1% Tween 20) and HRP-conjugated Goat Anti-Rabbit IgG (Proteintech; SA00001-2; 1:5,000 dilution in EveryBlot Blocking Buffer + 0.1% Tween 20). Blot was washed in PBS-T (0.1% Tween 20). Chemiluminescence was developed using SuperSignal West Pico PLUS Chemiluminescent Substrate (Thermo Fisher Scientific) and imaged using a ChemiDoc Plus Imaging System (BioRad). Quantification of the blot was performed with ImageLab software (version 6.1).

Human *CTSZ* analysis

We queried the summary statistics from a published genome-wide association study (GWAS) of TB severity in cases from Kampala, Uganda [61]. Briefly, two independent cohorts of culture-confirmed adult TB cases ($n = 149$, $n = 179$) [93] were included in a GWAS. TB severity was quantified using the Bandim TBscore, which enumerates TB symptoms (e.g., cough, hemoptysis, dyspnea) and clinical signs (e.g., anemia, low body mass index, high body temperature) [62,94]. SNPs within *CTSZ* were identified using a 5kb flanking region around the *CTSZ* start and end positions reported in Ensembl (GRCh38). Pairwise LD for these SNPs was evaluated as the squared inter-variant allele count correlations (R^2) using PLINK (version 1.90) in the larger of the two cohorts ($n = 179$). An LD plot was generated from these pairwise LD measures using the R package LDheatmap (version 1.0-5) [95]. The model used to estimate allele effects accounted for sex, HIV status, RNA-Seq batch, and genotypic principal components 1 and 2.

SNP eQTL assessment was performed for the four significant SNPs indicated in Table 1. A linear mixed effect model was developed in the R package kimma [96] to compare baseline, media, and *Mtb*-induced *CTSZ* expression against each SNP genotype. The eQTL model accounted for sex, HIV status, RNA-Seq batch, and genotypic principal components 1 and 2. *CTSZ* expression as $\log_2$ (counts per million) was obtained from RNA-Seq data normalized using voom [97]. RNA-Seq data used for these analyses originated from a previously published dataset of CD14+ monocytes isolated from individuals within the Uganda cohort [63]. Monocytes were subjected to 6-hour media or *Mtb* stimulation and transcriptionally assayed.

Statistical analysis and data visualization

Hypothesis testing was performed using R statistical software (version 4.3.1). Statistical tests used for hypothesis testing are noted in the figure legends. Shapiro–Wilks tests were used to assess normality in phenotype data prior to parametric hypothesis testing, and $\log_{10}$-transformation was applied for normalization where appropriate. Kaplan–Meier survival curves were calculated using the R package survminer (version 0.5.0). A visualization of mouse chromosome 2 was generated using the R package karyoploteR (version 1.16.0) from the GRCm38/mm10 mouse genome build. Heatmaps in Figs 1A and 2C were generated using the R packages ComplexHeatmap (version 2.21.2) and heatmaply (version 1.5.0), respectively. Optimization and sparse partial least squares discriminant analysis (sPLS-DA) on time course infection cohorts were performed on time point data using the R package mixOmics (version 6.24.0).

Supporting information

S1 Fig. Genetic validation and infection of *Ctsz*⁻/⁻ mice. (**A**) Expression of wildtype and truncated *Ctsz* in tail sections from B6, *Ctsz*⁺/⁻, and *Ctsz*⁻/⁻ mice. Approximate sizes of wildtype and truncated PCR products are indicated by black arrows. As previously described by Sevenich and colleagues, 2010 [91], exon 2 (containing the active site cysteine critical for the enzymatic activity of *Ctsz*), and a portion of intron 3 in *Ctsz* were deleted by homologous recombination and substituted by a cassette comprising an independent ribosomal entry sequence (IRES). External confirmation of these results was obtained by probing the *lacZ* reporter gene present in the inserted IRES vector. (**B**) Bacterial burden measured by dilution plating from spleen homogenate 4 weeks after aerosol infection with *Mtb* H37Rv ($n = 3–12$ per strain; all males except B6 and *Ctsz*⁻/⁻ groups, which included both sexes in equal proportion). Hypothesis testing was performed by one-way ANOVA and Dunnett's post hoc test on $\log_{10}$-transformed values. The data underlying this figure can be found in S1 Data sheet S1B.
(PDF)

S2 Fig. sPLS-DA and survival analysis comparing *Ctsz*⁻/⁻ and B6 mice. (**A**) Phenotype loadings contributing to sparse component 2. Mice were sacrificed at 2, 3, 4, and 8 weeks after aerosolized *Mtb* infection. Data are from two experiments with $n = 6–14$ mice per genotype, representative of both sexes, at each time point. Kaplan–Meier survival estimates of aerosol-infected B6 ($n = 23$) and *Ctsz*⁻/⁻ mice ($n = 62$) across two independent experiments, among (**B**) male and (**C**) female mice. Hypothesis testing was performed using a log-rank test. Equal proportions of both sexes were included. The data underlying this figure can be found in S1 Data sheets 2ABCDEF_S2A and 2G_S2BC.
(PDF)

S3 Fig. Minor alleles of *CTSZ* SNPs within the TB severity haplotype block are associated with lower TB severity score and significantly greater *CTSZ* expression. Comparison of TB severity, measured using Bandim TBScore, by genotype for (**A**) rs111630627, (**B**) rs8120779, and (**C**) rs76687632 SNPs. Expression of each allele of each SNP was assessed by RNA-Seq at 6 h after mock and *Mtb* infection in human-derived monocytes. *CTSZ* expression by monocytes harboring the minor allele for each SNP was significantly increased following both infection conditions for the (**D**) rs111630627, (**E**) rs8120779, and (**F**) rs76687632 SNPs. eQTL effects were assessed with a linear mixed effect model in kimma to account for sex, age, RNA-Seq batch, genotypic principal components 1 and 2, and kinship. The data underlying this figure can be found in S1 Data sheet 4CD_S3DEF.
(PDF)

S4 Fig. Cathepsin mRNA is highly expressed in human *Mtb* granuloma macrophages. (**A**) Heatmap depicting mRNA expression levels of several cathepsins and macrophage markers across unsupervised scRNA-Seq cell clusters. (**B**) The positional distribution of *CTSZ* expression in human *Mtb* granulomas as determined by Visium v2 spatial mRNA-Seq of Eosin-stained biopsy tissue sections from two patients with TB. This figure was generated by re-analysis of previously published data from Pyle and colleagues, 2025 [65]. Cell clusters were annotated by the authors. Data from Pyle and colleagues, 2025 are available in the NCBI GEO under accession numbers GSE296399 and GSE296400.
(PDF)

S1 File. Fig 1B raw image.
(TIF)

S2 File. S1A Fig raw image.
(PNG)

S1 Data. Source data for main and supporting figures.
(XLSX)

S1 Raw images. Annotated raw images for Fig 1B and S1A Fig.
(PDF)

S1 Table. Complete list of 81 *CTSZ* SNPs present in Ugandan household contact study cohorts and their associations with TB severity. TB severity was evaluated by Bandim TBScore. Summary statistics for the *CTSZ* variants shown are based on a meta-analysis of two independent cohorts of culture-confirmed adult TB cases (described in McHenry and colleagues, 2023 [61]). Each cohort utilized a linear regression model that controlled for HIV status, sex, and one principal component. Unadjusted *p*-values are reported. Abbreviations: CHR, chromosome; BP, base pair from GRCh38 build; MAF, minor allele frequency.
(XLSX)

Acknowledgments

Author contributions

Conceptualization: Rachel K. Meade, Dennis C. Ko, Thomas R. Hawn, David M. Tobin, Clare M. Smith.

Formal analysis: Rachel K. Meade, Erika J. Hughes, Joshua Ivie, Penelope H. Benchek.

Funding acquisition: Catherine M. Stein, Thomas R. Hawn, David M. Tobin, Clare M. Smith.

Investigation: Rachel K. Meade, Oyindamola O. Adefisayo, Marco T. P. Gontijo, Summer J. Harris, Charlie J. Pyle, Kaley M. Wilburn, Alwyn M. V. Ecker, Erika J. Hughes, Paloma D. Garcia, Joshua Ivie, Clare M. Smith.

Methodology: Clare M. Smith.

Project administration: Clare M. Smith.

Resources: Michael L. McHenry, Harriet Mayanja-Kizza, Jadee L. Neff, Jason E. Stout.

Software: Rachel K. Meade.

Supervision: Catherine M. Stein, Thomas R. Hawn, David M. Tobin, Clare M. Smith.

Validation: Oyindamola O. Adefisayo, Marco T. P. Gontijo.

Visualization: Charlie J. Pyle, Penelope H. Benchek.

Writing – original draft: Rachel K. Meade, Oyindamola O. Adefisayo, Marco T. P. Gontijo, Thomas R. Hawn, David M. Tobin, Clare M. Smith.

Writing – review & editing: Rachel K. Meade, Oyindamola O. Adefisayo, Marco T. P. Gontijo, Charlie J. Pyle, Kaley M. Wilburn, Alwyn M. V. Ecker, Erika J. Hughes, Paloma D. Garcia, Joshua Ivie, Penelope H. Benchek, Harriet Mayanja-Kizza, Jadee L. Neff, Dennis C. Ko, Jason E. Stout, Catherine M. Stein, Thomas R. Hawn, David M. Tobin, Clare M. Smith.

References

1. Sabin S, Herbig A, Vågene ÅJ, Ahlström T, Bozovic G, Arcini C, et al. A seventeenth-century *Mycobacterium tuberculosis* genome supports a Neolithic emergence of the *Mycobacterium tuberculosis* complex. Genome Biol. 2020;21(1):201. https://doi.org/10.1186/s13059-020-02112-1 PMID: 32778135

2. Ernst JD. The immunological life cycle of tuberculosis. Nat Rev Immunol. 2012;12(8):581–91. https://doi.org/10.1038/nri3259 PMID: 22790178

3. Horton KC, Richards AS, Emery JC, Esmail H, Houben RMGJ. Reevaluating progression and pathways following *Mycobacterium tuberculosis* infection within the spectrum of tuberculosis. Proc Natl Acad Sci U S A. 2023;120(47):e2221186120. https://doi.org/10.1073/pnas.2221186120 PMID: 37963250

4. Kallmann FJ, Reisner D. Twin studies on genetic variations in resistance to tuberculosis. J Hered. 1943;34(9):269–76. https://doi.org/10.1093/oxfordjournals.jhered.a105302

5. Simonds B. Tuberculosis in twins. London: Pitman; 1963.

6. Comstock GW. Tuberculosis in twins: a re-analysis of the Prophit survey. Am Rev Respir Dis. 1978;117(4):621–4. https://doi.org/10.1164/arrd.1978.117.4.621 PMID: 565607

7. Bellamy R, Ruwende C, Corrah T, McAdam KP, Whittle HC, Hill AV. Variations in the NRAMP1 gene and susceptibility to tuberculosis in West Africans. N Engl J Med. 1998;338(10):640–4. https://doi.org/10.1056/NEJM199803053381002 PMID: 9486992

8. Goldfeld AE, Delgado JC, Thim S, Bozon MV, Uglialoro AM, Turbay D, et al. Association of an HLA-DQ allele with clinical tuberculosis. JAMA. 1998;279(3):226–8. https://doi.org/10.1001/jama.279.3.226 PMID: 9438744

9. Bellamy R, Ruwende C, Corrah T, McAdam KP, Thursz M, Whittle HC, et al. Tuberculosis and chronic hepatitis B virus infection in Africans and variation in the vitamin D receptor gene. J Infect Dis. 1999;179(3):721–4. https://doi.org/10.1086/314614 PMID: 9952386

10. Wilkinson RJ, Llewelyn M, Toossi Z, Patel P, Pasvol G, Lalvani A, et al. Influence of vitamin D deficiency and vitamin D receptor polymorphisms on tuberculosis among Gujarati Asians in west London: a case-control study. Lancet. 2000;355(9204):618–21. https://doi.org/10.1016/S0140-6736(99)02301-6 PMID: 10696983

11. da Cruz HLA, da Silva RC, Segat L, de Carvalho MSZ de MG, Brandão LAC, Guimarães RL, et al. MBL2 gene polymorphisms and susceptibility to tuberculosis in a northeastern Brazilian population. Infect Genet Evol. 2013;19:323–9. https://doi.org/10.1016/j.meegid.2013.03.002 PMID: 23524205

12. Mhmoud N, Fahal A, Wendy van de Sande WJ. Association of IL-10 and CCL5 single nucleotide polymorphisms with tuberculosis in the Sudanese population. Trop Med Int Health. 2013;18(9):1119–27. https://doi.org/10.1111/tmi.12141 PMID: 23790189

13. Chen M, Liang Y, Li W, Wang M, Hu L, Abuaku BK, et al. Impact of MBL and MASP-2 gene polymorphism and its interaction on susceptibility to tuberculosis. BMC Infect Dis. 2015;15:151. https://doi.org/10.1186/s12879-015-0879-y PMID: 25887173

14. Nägler DK, Ménard R. Human cathepsin X: a novel cysteine protease of the papain family with a very short proregion and unique insertions. FEBS Lett. 1998;434(1–2):135–9. https://doi.org/10.1016/s0014-5793(98)00964-8 PMID: 9738465

15. Santamaría I, Velasco G, Pendás AM, Fueyo A, López-Otín C. Cathepsin Z, a novel human cysteine proteinase with a short propeptide domain and a unique chromosomal location. J Biol Chem. 1998;273(27):16816–23. https://doi.org/10.1074/jbc.273.27.16816 PMID: 9642240

16. Nägler DK, Zhang R, Tam W, Sulea T, Purisima EO, Ménard R. Human cathepsin X: a cysteine protease with unique carboxypeptidase activity. Biochemistry. 1999;38(39):12648–54. https://doi.org/10.1021/bi991371z PMID: 10504234

17. Sivaraman J, Nägler DK, Zhang R, Ménard R, Cygler M. Crystal structure of human procathepsin X: a cysteine protease with the proregion covalently linked to the active site cysteine. J Mol Biol. 2000;295(4):939–51. https://doi.org/10.1006/jmbi.1999.3410 PMID: 10656802

18. Guncar G, Klemencic I, Turk B, Turk V, Karaoglanovic-Carmona A, Juliano L, et al. Crystal structure of cathepsin X: a flip-flop of the ring of His23 allows carboxy-monopeptidase and carboxy-dipeptidase activity of the protease. Structure. 2000;8(3):305–13. https://doi.org/10.1016/s0969-2126(00)00108-8 PMID: 10745011

19. Deussing J, von Olshausen I, Peters C. Murine and human cathepsin Z: cDNA-cloning, characterization of the genes and chromosomal localization. Biochim Biophys Acta. 2000;1491(1–3):93–106. https://doi.org/10.1016/s0167-4781(00)00021-x PMID: 10760573

20. Therrien C, Lachance P, Sulea T, Purisima EO, Qi H, Ziomek E, et al. Cathepsins X and B can be differentiated through their respective mono- and dipeptidyl carboxypeptidase activities. Biochemistry. 2001;40(9):2702–11. https://doi.org/10.1021/bi002460a PMID: 11258881

21. Devanathan G, Turnbull JL, Ziomek E, Purisima EO, Ménard R, Sulea T. Carboxy-monopeptidase substrate specificity of human cathepsin X. Biochem Biophys Res Commun. 2005;329(2):445–52. https://doi.org/10.1016/j.bbrc.2005.01.150 PMID: 15737607

22. Dolenc I, Štefe I, Turk D, Taler-Verčič A, Turk B, Turk V, et al. Human cathepsin X/Z is a biologically active homodimer. Biochim Biophys Acta Proteins Proteom. 2021;1869(2):140567. https://doi.org/10.1016/j.bbapap.2020.140567 PMID: 33227497

23. Cooke GS, Campbell SJ, Bennett S, Lienhardt C, McAdam KPWJ, Sirugo G, et al. Mapping of a novel susceptibility locus suggests a role for MC3R and CTSZ in human tuberculosis. Am J Respir Crit Care Med. 2008;178(2):203–7. https://doi.org/10.1164/rccm.200710-1554OC PMID: 18420963

24. Adams LA, Möller M, Nebel A, Schreiber S, van der Merwe L, van Helden PD, et al. Polymorphisms in MC3R promoter and CTSZ 3′UTR are associated with tuberculosis susceptibility. Eur J Hum Genet. 2011;19(6):676–81. https://doi.org/10.1038/ejhg.2011.1 PMID: 21368909

25. Stein CM, Zalwango S, Malone LL, Won S, Mayanja-Kizza H, Mugerwa RD, et al. Genome scan of *M. tuberculosis* infection and disease in Ugandans. PLoS One. 2008;3(12):e4094. https://doi.org/10.1371/journal.pone.0004094 PMID: 19116662

26. Baker AR, Zalwango S, Malone LL, Igo RP Jr, Qiu F, Nsereko M, et al. Genetic susceptibility to tuberculosis associated with cathepsin Z haplotype in a Ugandan household contact study. Hum Immunol. 2011;72(5):426–30. https://doi.org/10.1016/j.humimm.2011.02.016 PMID: 21354459

27. Journet A, Chapel A, Kieffer S, Louwagie M, Luche S, Garin J. Towards a human repertoire of monocytic lysosomal proteins. Electrophoresis. 2000;21(16):3411–9. https://doi.org/10.1002/1522-2683(20001001)21:16<3411::aid-elps3411>3.0.co;2-m

28. Garin J, Diez R, Kieffer S, Dermine JF, Duclos S, Gagnon E, et al. The phagosome proteome: insight into phagosome functions. J Cell Biol. 2001;152(1):165–80. https://doi.org/10.1083/jcb.152.1.165 PMID: 11149929

29. Kos J, Jevnikar Z, Obermajer N. The role of cathepsin X in cell signaling. Cell Adh Migr. 2009;3(2):164–6. https://doi.org/10.4161/cam.3.2.7403 PMID: 19262176

30. Schmiedel BJ, Singh D, Madrigal A, Valdovino-Gonzalez AG, White BM, Zapardiel-Gonzalo J, et al. Impact of genetic polymorphisms on human immune cell gene expression. Cell. 2018;175(6):1701-1715.e16. https://doi.org/10.1016/j.cell.2018.10.022 PMID: 30449622

31. Obermajer N, Svajger U, Bogyo M, Jeras M, Kos J. Maturation of dendritic cells depends on proteolytic cleavage by cathepsin X. J Leukoc Biol. 2008;84(5):1306–15. https://doi.org/10.1189/jlb.0508285 PMID: 18701767

32. Jevnikar Z, Obermajer N, Bogyo M, Kos J. The role of cathepsin X in the migration and invasiveness of T lymphocytes. J Cell Sci. 2008;121(Pt 16):2652–61. https://doi.org/10.1242/jcs.023721 PMID: 18664495

33. Obermajer N, Repnik U, Jevnikar Z, Turk B, Kreft M, Kos J. Cysteine protease cathepsin X modulates immune response via activation of beta2 integrins. Immunology. 2008;124(1):76–88. https://doi.org/10.1111/j.1365-2567.2007.02740.x PMID: 18194276

34. Pires D, Marques J, Pombo JP, Carmo N, Bettencourt P, Neyrolles O, et al. Role of cathepsins in *Mycobacterium tuberculosis* survival in human macrophages. Sci Rep. 2016;6:32247. https://doi.org/10.1038/srep32247 PMID: 27572605

35. Lewis MS, Danelishvili L, Rose SJ, Bermudez LE. MAV_4644 interaction with the host cathepsin Z protects *Mycobacterium avium* subsp. *hominissuis* from rapid macrophage killing. Microorganisms. 2019;7(5):144. https://doi.org/10.3390/microorganisms7050144 PMID: 31117286

36. Saul MC, Philip VM, Reinholdt LG, Chesler EJ; Center for Systems Neurogenetics of Addiction. High-diversity mouse populations for complex traits. Trends Genet. 2019;35(7):501–14. https://doi.org/10.1016/j.tig.2019.04.003 PMID: 31133439

37. Villar-Hernández R, Ghodousi A, Konstantynovska O, Duarte R, Lange C, Raviglione M. Tuberculosis: current challenges and beyond. Breathe (Sheff). 2023;19(1):220166. https://doi.org/10.1183/20734735.0166-2022 PMID: 37334103

38. Medina E, North RJ. Evidence inconsistent with a role for the Bcg gene (Nramp1) in resistance of mice to infection with virulent *Mycobacterium tuberculosis*. J Exp Med. 1996;183(3):1045–51. https://doi.org/10.1084/jem.183.3.1045 PMID: 8642246

39. Medina E, North RJ. Resistance ranking of some common inbred mouse strains to *Mycobacterium tuberculosis* and relationship to major histocompatibility complex haplotype and Nramp1 genotype. Immunology. 1998;93(2):270–4. https://doi.org/10.1046/j.1365-2567.1998.00419.x PMID: 9616378

40. Green EL. Genetics and probability in animal breeding experiments. Macmillan Education UK. 1981. https://doi.org/10.1007/978-1-349-04904-2

41. Taylor BA, Heiniger HJ, Meier H. Genetic analysis of resistance to cadmium-induced testicular damage in mice. Proc Soc Exp Biol Med. 1973;143(3):629–33. https://doi.org/10.3181/00379727-143-37380 PMID: 4719448

42. Taylor BA, Wnek C, Kotlus BS, Roemer N, MacTaggart T, Phillips SJ. Genotyping new BXD recombinant inbred mouse strains and comparison of BXD and consensus maps. Mamm Genome. 1999;10(4):335–48. https://doi.org/10.1007/s003359900998 PMID: 10087289

43. Peirce JL, Lu L, Gu J, Silver LM, Williams RW. A new set of BXD recombinant inbred lines from advanced intercross populations in mice. BMC Genet. 2004;5:7. https://doi.org/10.1186/1471-2156-5-7 PMID: 15117419

44. Ashbrook DG, Arends D, Prins P, Mulligan MK, Roy S, Williams EG, et al. A platform for experimental precision medicine: the extended BXD mouse family. Cell Syst. 2021;12(3):235-247.e9. https://doi.org/10.1016/j.cels.2020.12.002 PMID: 33472028

45. Churchill GA, Airey DC, Allayee H, Angel JM, Attie AD, Beatty J, et al. The collaborative cross, a community resource for the genetic analysis of complex traits. Nat Genet. 2004;36(11):1133–7. https://doi.org/10.1038/ng1104-1133 PMID: 15514660

46. Collaborative Cross Consortium. The genome architecture of the collaborative cross mouse genetic reference population. Genetics. 2012;190(2):389–401. https://doi.org/10.1534/genetics.111.132639 PMID: 22345608

47. Srivastava A, Morgan AP, Najarian ML, Sarsani VK, Sigmon JS, Shorter JR, et al. Genomes of the mouse collaborative cross. Genetics. 2017;206(2):537–56. https://doi.org/10.1534/genetics.116.198838 PMID: 28592495

48. Meade RK, Smith CM. Immunological roads diverged: mapping tuberculosis outcomes in mice. Trends Microbiol. 2025;33(1):15–33. https://doi.org/10.1016/j.tim.2024.06.007 PMID: 39034171

49. Meade RK, Long JE, Jinich A, Rhee KY, Ashbrook DG, Williams RW, et al. Genome-wide screen identifies host loci that modulate *Mycobacterium tuberculosis* fitness in immunodivergent mice. G3 (Bethesda). 2023;13(9):jkad147. https://doi.org/10.1093/g3journal/jkad147 PMID: 37405387

50. Smith CM, Baker RE, Proulx MK, Mishra BB, Long JE, Park SW, et al. Host-pathogen genetic interactions underlie tuberculosis susceptibility in genetically diverse mice. Elife. 2022;11:e74419. https://doi.org/10.7554/eLife.74419 PMID: 35112666

51. Koyuncu D, Niazi MKK, Tavolara T, Abeijon C, Ginese ML, Liao Y, et al. CXCL1: a new diagnostic biomarker for human tuberculosis discovered using diversity outbred mice. PLoS Pathog. 2021;17(8):e1009773. https://doi.org/10.1371/journal.ppat.1009773 PMID: 34403447

52. Ahmed M, Thirunavukkarasu S, Rosa BA, Thomas KA, Das S, Rangel-Moreno J, et al. Immune correlates of tuberculosis disease and risk translate across species. Sci Transl Med. 2020;12(528):eaay0233. https://doi.org/10.1126/scitranslmed.aay0233 PMID: 31996462

53. Moreira-Teixeira L, Tabone O, Graham CM, Singhania A, Stavropoulos E, Redford PS, et al. Mouse transcriptome reveals potential signatures of protection and pathogenesis in human tuberculosis. Nat Immunol. 2020;21(4):464–76. https://doi.org/10.1038/s41590-020-0610-z PMID: 32205882

54. Zak DE, Penn-Nicholson A, Scriba TJ, Thompson E, Suliman S, Amon LM, et al. A blood RNA signature for tuberculosis disease risk: a prospective cohort study. Lancet. 2016;387(10035):2312–22. https://doi.org/10.1016/S0140-6736(15)01316-1 PMID: 27017310

55. Adams DJ, Doran AG, Lilue J, Keane TM. The Mouse Genomes Project: a repository of inbred laboratory mouse strain genomes. Mamm Genome. 2015;26(9–10):403–12. https://doi.org/10.1007/s00335-015-9579-6 PMID: 26123534

56. Desvignes L, Wolf AJ, Ernst JD. Dynamic roles of type I and type II IFNs in early infection with *Mycobacterium tuberculosis*. J Immunol. 2012;188(12):6205–15. https://doi.org/10.4049/jimmunol.1200255 PMID: 22566567

57. Wolf AJ, Desvignes L, Linas B, Banaiee N, Tamura T, Takatsu K, et al. Initiation of the adaptive immune response to *Mycobacterium tuberculosis* depends on antigen production in the local lymph node, not the lungs. J Exp Med. 2008;205(1):105–15. https://doi.org/10.1084/jem.20071367 PMID: 18158321

58. Gopal R, Monin L, Torres D, Slight S, Mehra S, McKenna KC, et al. S100A8/A9 proteins mediate neutrophilic inflammation and lung pathology during tuberculosis. Am J Respir Crit Care Med. 2013;188(9):1137–46. https://doi.org/10.1164/rccm.201304-0803OC PMID: 24047412

59. Cronan MR, Hughes EJ, Brewer WJ, Viswanathan G, Hunt EG, Singh B, et al. A non-canonical type 2 immune response coordinates tuberculous granuloma formation and epithelialization. Cell. 2021;184(7):1757-1774.e14. https://doi.org/10.1016/j.cell.2021.02.046 PMID: 33761328

60. Gideon HP, Hughes TK, Tzouanas CN, Wadsworth MH 2nd, Tu AA, Gierahn TM, et al. Multimodal profiling of lung granulomas in macaques reveals cellular correlates of tuberculosis control. Immunity. 2022;55(5):827-846.e10. https://doi.org/10.1016/j.immuni.2022.04.004 PMID: 35483355

61. McHenry ML, Simmons J, Hong H, Malone LL, Mayanja-Kizza H, Bush WS, et al. Tuberculosis severity associates with variants and eQTLs related to vascular biology and infection-induced inflammation. PLoS Genet. 2023;19(3):e1010387. https://doi.org/10.1371/journal.pgen.1010387 PMID: 36972313

62. Rudolf F. The Bandim TBscore—reliability, further development, and evaluation of potential uses. Glob Health Action. 2014;7:24303. https://doi.org/10.3402/gha.v7.24303 PMID: 24857613

63. Simmons JD, Dill-McFarland KA, Stein CM, Van PT, Chihota V, Ntshiqa T, et al. Monocyte transcriptional responses to *Mycobacterium tuberculosis* associate with resistance to tuberculin skin test and interferon gamma release assay conversion. mSphere. 2022;7(3):e0015922. https://doi.org/10.1128/msphere.00159-22 PMID: 35695527

64. Yanai I, Benjamin H, Shmoish M, Chalifa-Caspi V, Shklar M, Ophir R, et al. Genome-wide midrange transcription profiles reveal expression level relationships in human tissue specification. Bioinformatics. 2005;21(5):650–9. https://doi.org/10.1093/bioinformatics/bti042 PMID: 15388519

65. Pyle CJ, Wang L, Beerman RW, Jain V, Ohman HKE, Thompson BA, et al. Paired single-cell and spatial transcriptional profiling reveals a central osteopontin macrophage response mediating tuberculous granuloma formation. mBio. 2025:e0155925. https://doi.org/10.1128/mbio.01559-25 PMID: 40772762

66. Cronan MR. In the thick of it: formation of the tuberculous granuloma and its effects on host and therapeutic responses. Front Immunol. 2022;13:820134. https://doi.org/10.3389/fimmu.2022.820134 PMID: 35320930

67. Obermajer N, Premzl A, Zavasnik Bergant T, Turk B, Kos J. Carboxypeptidase cathepsin X mediates beta2-integrin-dependent adhesion of differentiated U-937 cells. Exp Cell Res. 2006;312(13):2515–27. https://doi.org/10.1016/j.yexcr.2006.04.019 PMID: 16774752

68. Augenstreich J, Haanappel E, Sayes F, Simeone R, Guillet V, Mazeres S, et al. Phthiocerol dimycocerosates from *Mycobacterium tuberculosis* increase the membrane activity of bacterial effectors and host receptors. Front Cell Infect Microbiol. 2020;10:420. https://doi.org/10.3389/fcimb.2020.00420 PMID: 32923411

69. Boro M, Balaji KN. CXCL1 and CXCL2 regulate NLRP3 inflammasome activation via G-protein–coupled receptor CXCR2. J Immunol. 2017;199(5):1660–71. https://doi.org/10.4049/jimmunol.1700129 PMID: 28739876

70. Keller C, Hoffmann R, Lang R, Brandau S, Hermann C, Ehlers S. Genetically determined susceptibility to tuberculosis in mice causally involves accelerated and enhanced recruitment of granulocytes. Infect Immun. 2006;74(7):4295–309. https://doi.org/10.1128/IAI.00057-06 PMID: 16790804

71. Krueger S, Bernhardt A, Kalinski T, Baldensperger M, Zeh M, Teller A, et al. Induction of premalignant host responses by cathepsin x/z-deficiency in *Helicobacter pylori*-infected mice. PLoS One. 2013;8(7):e70242. https://doi.org/10.1371/journal.pone.0070242 PMID: 23936173

72. Haist M, Ries F, Gunzer M, Bednarczyk M, Siegel E, Kuske M, et al. Neutrophil-specific knockdown of β2 integrins impairs antifungal effector functions and aggravates the course of invasive pulmonal aspergillosis. Front Immunol. 2022;13:823121. https://doi.org/10.3389/fimmu.2022.823121 PMID: 35734179

73. Jevnikar Z, Obermajer N, Pecar-Fonović U, Karaoglanovic-Carmona A, Kos J. Cathepsin X cleaves the β2 cytoplasmic tail of LFA-1 inducing the intermediate affinity form of LFA-1 and α-actinin-1 binding. Eur J Immunol. 2009;39(11):3217–27. https://doi.org/10.1002/eji.200939562 PMID: 19750481

74. Jevnikar Z, Obermajer N, Doljak B, Turk S, Gobec S, Svajger U, et al. Cathepsin X cleavage of the β_2 integrin regulates talin-binding and LFA-1 affinity in T cells. J Leukoc Biol. 2011;90(1):99–109. https://doi.org/10.1189/jlb.1110622 PMID: 21454358

75. Gupta M, Srikrishna G, Klein SL, Bishai WR. Genetic and hormonal mechanisms underlying sex-specific immune responses in tuberculosis. Trends Immunol. 2022;43(8):640–56. https://doi.org/10.1016/j.it.2022.06.004 PMID: 35842266

76. Barcena ML, Niehues MH, Christiansen C, Estepa M, Haritonow N, Sadighi AH, et al. Male macrophages and fibroblasts from C57/BL6J mice are more susceptible to inflammatory stimuli. Front Immunol. 2021;12:758767. https://doi.org/10.3389/fimmu.2021.758767 PMID: 34867999

77. Krueger S, Kalinski T, Hundertmark T, Wex T, Küster D, Peitz U, et al. Up-regulation of cathepsin X in *Helicobacter pylori* gastritis and gastric cancer. J Pathol. 2005;207(1):32–42. https://doi.org/10.1002/path.1820 PMID: 16025436

78. Selkrig J, Li N, Hausmann A, Mangan MSJ, Zietek M, Mateus A, et al. Spatiotemporal proteomics uncovers cathepsin-dependent macrophage cell death during *Salmonella* infection. Nat Microbiol. 2020;5(9):1119–33. https://doi.org/10.1038/s41564-020-0736-7 PMID: 32514074

79. Wendt W, Zhu X-R, Lübbert H, Stichel CC. Differential expression of cathepsin X in aging and pathological central nervous system of mice. Exp Neurol. 2007;204(2):525–40. https://doi.org/10.1016/j.expneurol.2007.01.007 PMID: 17306794

80. Kraus S, Bunsen T, Schuster S, Cichoń MA, Tacke M, Reinheckel T, et al. Cellular senescence induced by cathepsin X downregulation. Eur J Cell Biol. 2011;90(8):678–86. https://doi.org/10.1016/j.ejcb.2011.03.008 PMID: 21616554

81. Allan ERO, Campden RI, Ewanchuk BW, Tailor P, Balce DR, McKenna NT, et al. A role for cathepsin Z in neuroinflammation provides mechanistic support for an epigenetic risk factor in multiple sclerosis. J Neuroinflammation. 2017;14(1):103. https://doi.org/10.1186/s12974-017-0874-x PMID: 28486971

82. Nishida N, Aiba Y, Hitomi Y, Kawashima M, Kojima K, Kawai Y, et al. NELFCD and CTSZ loci are associated with jaundice-stage progression in primary biliary cholangitis in the Japanese population. Sci Rep. 2018;8(1):8071. https://doi.org/10.1038/s41598-018-26369-6 PMID: 29795304

83. Aiba Y, Harada K, Ito M, Suematsu T, Aishima S, Hitomi Y, et al. Increased expression and altered localization of cathepsin Z are associated with progression to jaundice stage in primary biliary cholangitis. Sci Rep. 2018;8(1):11808. https://doi.org/10.1038/s41598-018-30146-w PMID: 30087368

84. Dera AA, Ranganath L, Barraclough R, Vinjamuri S, Hamill S, Barraclough DL. Cathepsin Z as a novel potential biomarker for osteoporosis. Sci Rep. 2019;9(1):9752. https://doi.org/10.1038/s41598-019-46068-0 PMID: 31278293

85. Hafner A, Glavan G, Obermajer N, Živin M, Schliebs R, Kos J. Neuroprotective role of γ-enolase in microglia in a mouse model of Alzheimer's disease is regulated by cathepsin X. Aging Cell. 2013;12(4):604–14. https://doi.org/10.1111/acel.12093 PMID: 23621429

86. Olson OC, Joyce JA. Cysteine cathepsin proteases: regulators of cancer progression and therapeutic response. Nat Rev Cancer. 2015;15(12):712–29. https://doi.org/10.1038/nrc4027 PMID: 26597527

87. Li J, Zhou X, Li L, Ji L, Li J, Qu Y, et al. The association between CTSZ methylation in peripheral blood and breast cancer in Chinese women. Front Oncol. 2023;13:1148635. https://doi.org/10.3389/fonc.2023.1148635 PMID: 37274256

88. Vizin T, Christensen IJ, Nielsen HJ, Kos J. Cathepsin X in serum from patients with colorectal cancer: relation to prognosis. Radiol Oncol. 2012;46(3):207–12. https://doi.org/10.2478/v10019-012-0040-0 PMID: 23077459

89. Nägler DK, Krüger S, Kellner A, Ziomek E, Menard R, Buhtz P, et al. Up-regulation of cathepsin X in prostate cancer and prostatic intraepithelial neoplasia. Prostate. 2004;60(2):109–19. https://doi.org/10.1002/pros.20046 PMID: 15162377

90. Wang J, Chen L, Li Y, Guan X-Y. Overexpression of cathepsin Z contributes to tumor metastasis by inducing epithelial-mesenchymal transition in hepatocellular carcinoma. PLoS One. 2011;6(9):e24967. https://doi.org/10.1371/journal.pone.0024967 PMID: 21966391

91. Sevenich L, Schurigt U, Sachse K, Gajda M, Werner F, Müller S, et al. Synergistic antitumor effects of combined cathepsin B and cathepsin Z deficiencies on breast cancer progression and metastasis in mice. Proc Natl Acad Sci U S A. 2010;107(6):2497–502. https://doi.org/10.1073/pnas.0907240107 PMID: 20133781

92. Wang J, Sha J, Strong E, Chopra AK, Lee S. FDA-approved amoxapine effectively promotes macrophage control of mycobacteria by inducing autophagy. Microbiol Spectr. 2022;10(5):e0250922. https://doi.org/10.1128/spectrum.02509-22 PMID: 36129262

93. Stein CM, Zalwango S, Malone LL, Thiel B, Mupere E, Nsereko M, et al. Resistance and susceptibility to *Mycobacterium tuberculosis* infection and disease in tuberculosis households in Kampala, Uganda. Am J Epidemiol. 2018;187(7):1477–89. https://doi.org/10.1093/aje/kwx380 PMID: 29304247

94. Wejse C, Gustafson P, Nielsen J, Gomes VF, Aaby P, Andersen PL, et al. TBscore: signs and symptoms from tuberculosis patients in a low-resource setting have predictive value and may be used to assess clinical course. Scand J Infect Dis. 2008;40(2):111–20. https://doi.org/10.1080/00365540701558698 PMID: 17852907

95. Shin J-H, Blay S, Graham J, McNeney B. LDheatmap: an R function for graphical display of pairwise linkage disequilibria between single nucleotide polymorphisms. J Stat Soft. 2006;16(Code Snippet 3). https://doi.org/10.18637/jss.v016.c03

96. Dill-McFarland KA, Mitchell K, Batchu S, Segnitz RM, Benson B, Janczyk T, et al. Kimma: flexible linear mixed effects modeling with kinship covariance for RNA-seq data. Bioinformatics. 2023;39(5):btad279. https://doi.org/10.1093/bioinformatics/btad279 PMID: 37140544

97. Law CW, Chen Y, Shi W, Smyth GK. voom: precision weights unlock linear model analysis tools for RNA-seq read counts. Genome Biol. 2014;15(2):R29. https://doi.org/10.1186/gb-2014-15-2-r29 PMID: 24485249